

## ARTICLE OPEN



# High yield manufacturing of fully screen-printed organic electrochemical transistors

Marzieh Zabihipour<sup>1</sup>, Roman Lassnig<sup>2</sup>, Jan Strandberg<sup>2</sup>, Magnus Berggren<sup>1</sup>, Simone Fabiano<sup>1</sup>, Isak Engquist<sup>1</sup>✉ and Peter Andersson Ersman<sup>2</sup>

The potential of the screen printing method for large-scale production of organic electrochemical transistors (OECTs), combining high production yield with low cost, is here demonstrated. Fully screen-printed OECTs of 1 mm<sup>2</sup> area, based on poly(3,4-ethylenedioxythiophene) doped with poly(styrenesulfonate) (PEDOT:PSS), have been manufactured on flexible polyethylene terephthalate (PET) substrates. The goal of this project effort has been to explore and develop the printing processing to enable high yield and stable transistor parameters, targeting miniaturized digital OECT circuits for large-scale integration (LSI). Of the 760 OECTs manufactured in one batch on a PET sheet, only two devices were found malfunctioning, thus achieving an overall manufacturing yield of 99.7%. A drain current ON/OFF ratio at least equal to 400 was applied as the strict exclusion principle for the yield, motivated by proper operation in LSI circuits. This consistent performance of low-footprint OECTs allows for the integration of PEDOT:PSS-based OECTs into complex logic circuits operating at high stability and accuracy.

npj Flexible Electronics (2020)4:15; <https://doi.org/10.1038/s41528-020-0078-9>

## INTRODUCTION

Printed electronics enables high volume production of thin and flexible sensor and communication technology at low cost<sup>1</sup>. The technology is an enabler for various Internet of Things and bioelectronics applications, such as sensors, drug delivery, and communication outposts that offer advanced functionality in an embedded and highly distributed fashion<sup>2</sup>. Over the years, several archetypical techniques have been established within the printed electronics community to process and produce a vast array of functional materials<sup>1</sup>, needed to achieve devices and systems, where the screen printing technique is one of the most commonly used methods<sup>1,3–7</sup>. In the screen printing process, the ink is squeezed through the open areas of the patterned mesh, which allows reproduction of configurations on a wide variety of surfaces (rough, planar, bent, stretchable etc.) and materials, e.g., paper, plastics, cardboard, wood, etc<sup>8</sup>. Printed electronic devices, which commonly are based on multi-layered device architectures, are realized by printing different functional layers onto the substrate. In a complete layout of a full circuit design each layer is realized using a unique mesh and pattern. The manufacturing is done layer by layer and the functionality and overall performance of the resulting components are heavily dependent on the alignment and patterning accuracy of every individual layer.

An organic electrochemical transistor (OECT) is a three terminal device in which the drain and source electrodes are connected via an organic semiconducting polymer, serving as the transistor channel, and the third electrode (gate) is separated from the channel by an electrolyte. Thus, the source and drain electrodes are electronically connected, via the channel, while the gate electrode and the channel are ionically connected. This allows for polarization of the gate and channel that causes charge accumulation/depletion of the channel, which is driven by the application of a gate-source voltage. OECTs were first introduced by Mark S. Wrighton in 1984<sup>9</sup> and were later, especially with the advent of poly(styrene sulfonate)-doped poly(3,4-ethylenedioxythiophene)

(PEDOT:PSS)<sup>10</sup>, improved and further developed<sup>8</sup>. When complexed with PSS, PEDOT is oxidized and highly conducting<sup>11</sup> and may be switched to its semiconducting state when reduced to its neutral state via the exchange of cations. Hence, PEDOT-PSS-based OECTs are switched from “ON” to “OFF” upon the application of a gate voltage; it is a p-type depletion mode transistor.

In the last decade, the development of OECTs has rapidly evolved and the technology has found its way into applications in, e.g., printed electronics and bioelectronics, exemplified by digital logic circuits<sup>5</sup>, smart textiles<sup>12</sup>, electrochromic active-matrix displays<sup>13</sup>, neuromorphic computing<sup>14</sup>, biosensing<sup>15</sup>, and neuronal recordings<sup>16</sup>. In those applications, the key advantages of the OECT technology are utilized, exemplified by simple device architecture, robustness while operated in ambient or aqueous media, easy and additive manufacturing protocols, low operational voltage, and compatibility with flexible/rough/stretchable and large-area substrates<sup>4</sup>.

In all OECT applications, and in particular for OECT-based integrated logic circuits, predictable and stable operation of every single standalone OECT is crucial. For example, in the case of printing a logic circuit composed of 100 OECTs, a minimum OECT manufacturing yield of 99.3% must be attained in order to guarantee an average resulting functional yield of 50% for the complete circuits, whereas an OECT manufacturing yield of 85–90% leads to no operational circuits at all. Even though many studies have focused on printed organic (electrochemical) transistors and circuits<sup>3,5,7,13</sup>, the manufacturing yield and performance statistics of such devices and circuits are rather unexplored. Sowade et al.<sup>17</sup> have reported on the manufacturing of 924 all-inkjet-printed organic thin film transistors (OTFTs) arranged in six arrays, each including 154 TFTs. The yield, studied in terms of the transistor ON/OFF current ratio, ranges from 69% for the best performing array down to 6% for the array performing worst, with a yield value strongly correlated to the position of the arrays along the substrate<sup>17</sup>. In a second report, the same team

<sup>1</sup>Laboratory of Organic Electronics, Department of Science and Technology, Linköping University, SE-601 74, Norrköping, Sweden. <sup>2</sup>RISE Research Institutes of Sweden, Printed, Bio- and Organic Electronics, Bredgatan 33, SE-602 21, Norrköping, Sweden. ✉email: [isak.engquist@liu.se](mailto:isak.engquist@liu.se)

reported on the improvement of the yield of OTFTs, again using inkjet printing as the production method<sup>18</sup>. In that report, the functional OTFTs were classified as operational devices if the ON/OFF current ratio was >200, which resulted in a maximum OTFT manufacturing yield of 82%. Studies of the manufacturing yield of screen-printed OECTs has so far not been reported.

Here, we report the investigation of the manufacturing yield and operational statistics of PEDOT:PSS-based screen-printed OECTs. The OECTs were manufactured solely using flatbed screen printing, a choice that was motivated by a desire for a robust and cost-effective production protocol. Since the PEDOT:PSS-based OECTs are p-type depletion mode transistors, a gate voltage close to 0 V results in a high drain current, thus the OECT is said to operate in its ON state. The operation of OECTs is based on volumetric gating of the channel, hence, when a positive gate voltage is applied, vs. the source and channel potential, cations from the electrolyte enter the PEDOT:PSS channel to compensate the sulfonate anions of the PSS. This causes a reduction of the PEDOT polymer chains<sup>19</sup> and a de-doping of the OECT channel towards its OFF state. By consecutively switching the potential of the gate in between different voltages, reversible exchange of ions with the electrolyte takes place, which forces the channel to undergo reversible modulation of its doping state through its entire volume<sup>5</sup>. The electrolyte gating allows for low-voltage operation; a gate voltage below 1.5 V is sufficient to “fully” switch OFF the channel. In this work, the OECTs have been manufactured by screen printing on flexible polyethylene terephthalate (PET) substrates in ambient conditions, and the printed inks were either UV-cured or thermally cured at a maximum temperature of 120 °C. The fabricated vertical OECTs are built up from five different screen printable materials: silver, PEDOT:PSS, carbon, electrolyte, and an insulating material. Three different OECT structures were designed and investigated, and their performances have been examined with respect to their ON/OFF current ratios. Our findings demonstrate the potential of using screen-printed OECTs in complex digital circuitry.

## RESULTS

The impact of OECT channel size on performance and yield

The performance of the printed OECTs was evaluated using the ON/OFF current ratio as one prime figure of merit for transistor current modulation. The ON/OFF current ratio is one of the most crucial transistor parameters and is of great importance as it impacts the logic switching characteristics in digital circuits. In one full print run, a total number of 760 OECTs are manufactured on a ~A4-sized substrate area (200 × 300 mm<sup>2</sup>, Fig. 1). Statistical investigations of the device performance are essential in order to determine the ON/OFF-based yield as a function of OECT design. Moreover, from a digital circuitry standpoint, only 20% of the total area of the printed A4-sized sheet is required to realize complex circuits such as decoders and shift registers<sup>20</sup>, circuits which typically consist of more than 100 OECTs. In this study we evaluate, in depth, all the OECTs printed onto one single sheet, even though one print batch typically contains an (statistical) ensemble of several sheets. We expect the variation between sheets to be very small since the most crucial fabrication step, the alignment between layers, was tuned for every sheet with respect to the alignment marks of the previously printed layers. Besides the ON/OFF current ratio vs. OECT design, our investigation will also provide information about the quality of the screen printing process across the total substrate area, by determining the variation of the ON/OFF current ratio vs. the OECT location on the particular sheet. The test design includes 120 blocks, where each block contains five OECTs and each OECT has a channel area of 200 × 200 μm<sup>2</sup> (referred to as Small OECTs). Additionally, the design contains 32 blocks of five relatively larger sized OECTs, with a channel dimension of 400 × 400 μm<sup>2</sup> (referred to as Large OECTs). In total, 600 Small OECTs and 160 Large OECTs are available on the full test design.

For all OECTs studied, two carbon features serve as the source and drain electrodes, i.e., injecting and extracting holes transported through the PEDOT channel, respectively (Fig. 2). A rectangular area of each carbon contact is not covered by any insulator layer and is therefore also in direct contact with the electrolyte layer. The Small OECT structure has a total carbon area

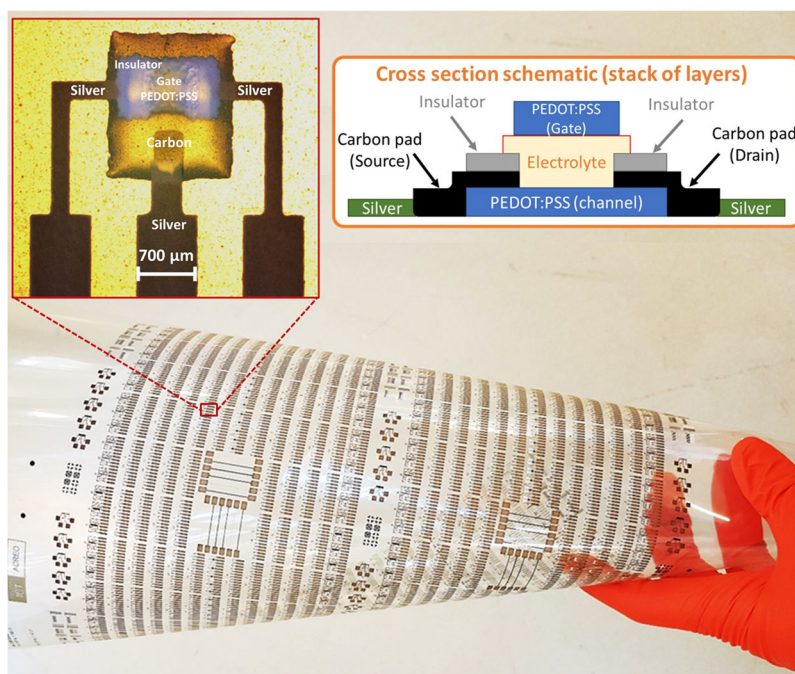


**Fig. 1** Screen-printed OECTs. A screen-printed sheet containing 760 OECTs, a microscope image of a single OECT, and a cross-section schematic illustrating the different material layers of the OECT architecture.

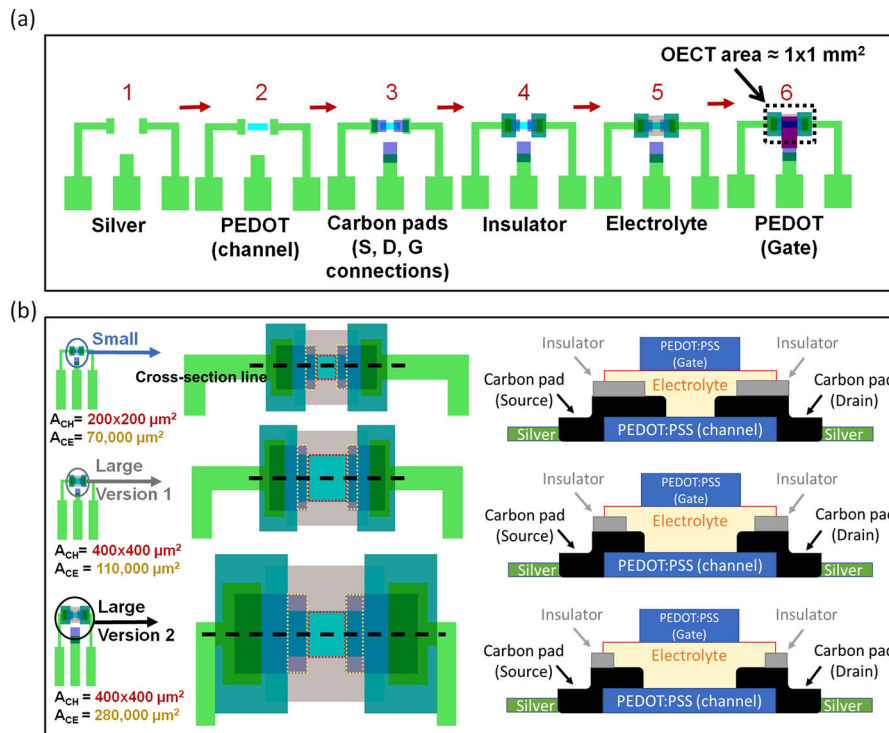


**Fig. 2 Detailed schematics of OECT layouts.** **a** Sequence of six printed layers and the approximate footprint per OECT, **b** three different OECT architectures with different channel areas ( $A_{CH}$  indicated via red dashed squares) and carbon areas exposed to the electrolyte ( $A_{CE}$  indicated via yellow dashed rectangles) are shown with the corresponding top and cross-sectional views for each OECT geometry. The multi-layered stacks in the cross-sectional views are schematically showing how channel length and  $A_{CE}$  vary for the three OECT designs.

of  $70,000 \mu\text{m}^2$  that is exposed to the electrolyte. The large OECTs are divided into two kinds: (i) large OECTs with a  $110,000 \mu\text{m}^2$  carbon area exposed to the electrolyte: referred to as Large Version 1; and (ii) large OECTs with an exposed carbon area of  $280,000 \mu\text{m}^2$ : referred to as Large Version 2. The purpose of designing two sets of large OECTs is to study the effect of the carbon area exposed to the electrolyte while keeping the channel dimensions (OECT size) constant. Therefore, the layout includes three sets of OECT structures (Small, Large Version 1, Large Version 2). Top and cross-sectional views of the OECT structures are given in Fig. 1. The complete screen printing process to manufacture the OECTs is given in Fig. 2a. The approximate footprint of a single OECT, omitting any conducting routing lines, measures  $\sim 1 \times 1 \text{ mm}^2$  (marked with a dashed square in the figure). In Fig. 2b, the three OECT structures are depicted; yellow rectangles illustrate the carbon contacts exposed to the electrolyte and red squares mark the active channel areas.

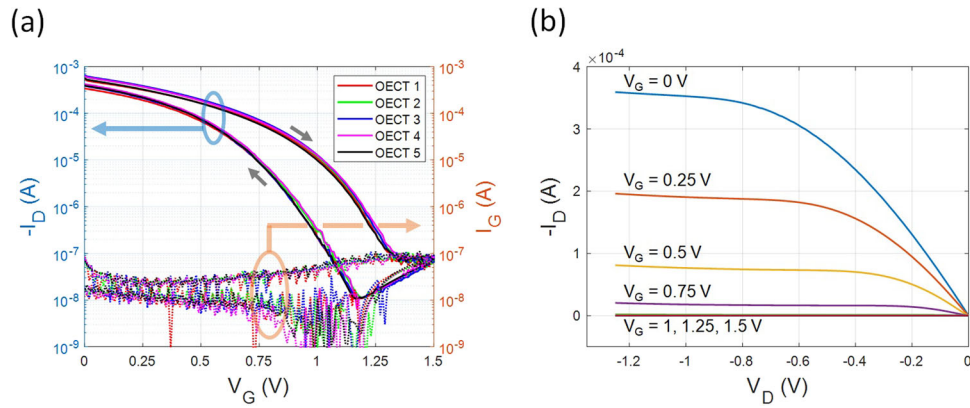
All 760 OECTs were evaluated by measuring the ON/OFF current ratio. Figure 3 shows typical transfer and output characteristics, respectively, for a block of five adjacent Small OECTs. While measuring the transfer characteristics, a fixed  $V_D = -1 \text{ V}$  was applied while  $V_G$  was swept from  $0 \rightarrow 1.5 \rightarrow 0 \text{ V}$  by using a voltage step of  $10 \text{ mV}$ . In the output measurements,  $V_D$  was swept from  $0$  to  $-1.25 \text{ V}$  by using a voltage step of  $10 \text{ mV}$ , for  $V_G$  values ranging from  $0$  to  $1.5 \text{ V}$  with  $250 \text{ mV}$  increments. For all measurements, an integration time of  $20 \text{ ms}$  was used for each data point.

The results in Fig. 3a show that the ON/OFF ( $I_D(V_G = 0)/I_D(V_G = 1.5 \text{ V})$ ) current modulation reaches approximately 10,000 for the Small OECTs. The gate current ( $I_{G,OFF}$ ) equals  $I_{D,OFF}$  as the PEDOT phase in the channel is “fully” reduced close to its neutral state (at  $V_G > 1.3 \text{ V}$ ). For the transfer curve measurements  $I_{D,ON}$  and  $I_{D,OFF}$  are picked from the forward sweep, the latter value is picked at  $V_G$  equal to  $1.5 \text{ V}$ . The channel includes a capacitive component that will result in an initial current drop, which is caused by a potential gradient along the channel upon applying  $V_D$ . Therefore, to avoid

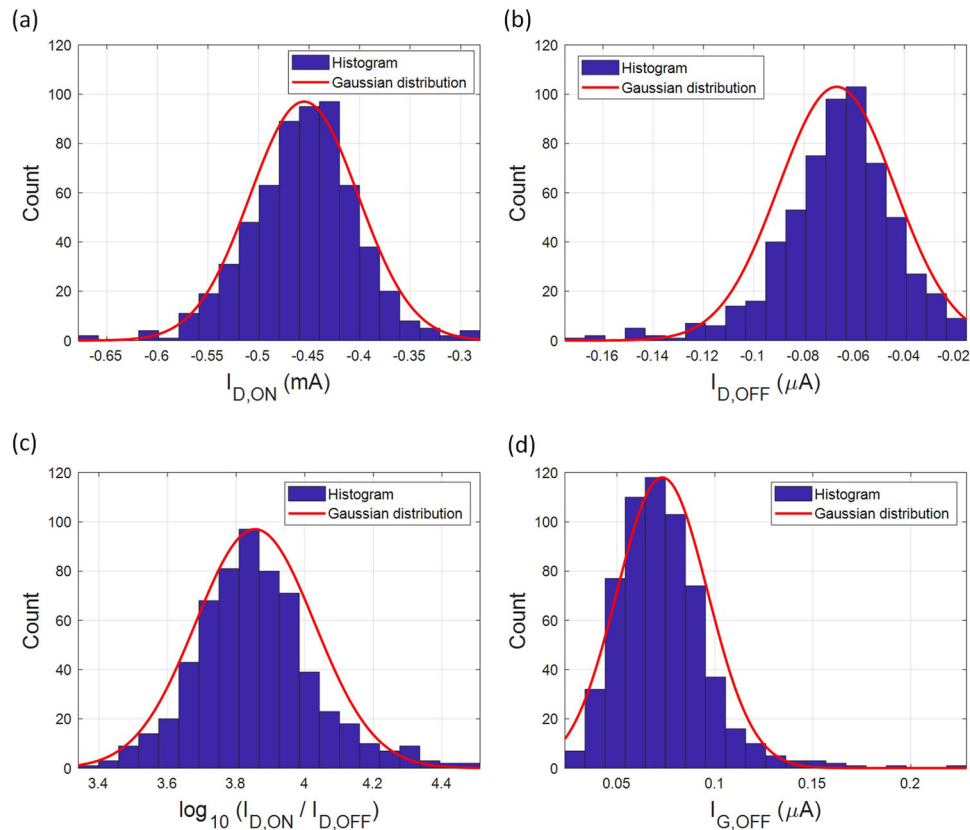
such initial capacitive-like behavior in the ON/OFF current ratio estimations,  $I_{D,ON}$  values were extracted at  $V_G$  equal to  $0.1 \text{ V}$ . Figure 3b shows the typical output characteristics of the Small OECTs where the linear (low  $V_D$ ) and saturated (elevated  $V_D$ ) regimes are clearly observed for different  $V_G$  values.

Figure 4 includes the histograms of the  $I_{D,ON}$ ,  $I_{D,OFF}$ ,  $I_{G,OFF}$  values and the drain current ON/OFF ratio for all the 600 Small OECTs recorded from the forward sweeps of each transfer curve. The empirical mean values of  $I_{D,ON}$ ,  $I_{D,OFF}$ ,  $I_{G,OFF}$ , and the ON/OFF current ratio is  $-0.4 \text{ mA}$ ,  $-70 \text{ nA}$ ,  $73 \text{ nA}$ , and 7800, respectively. Based on these empirical mean values and corresponding standard deviations, Gaussian distributions are given. The OECTs, here studied, are designed and aimed to be used in circuits. Circuits relying on p-type depletion mode OECTs are typically based on the concept of voltage division in a resistor ladder ( $R_1$ ,  $R_2$ ,  $R_3$ ), and it is assumed that a functional circuit requires at least a channel resistance that can be switched between values that are  $\sim 20$  times lower (ON) and  $\sim 20$  times higher (OFF) than the value of a specific resistor ( $R_3$ ) in the ladder. Hence, a minimum ON/OFF current ratio of  $\sim 400$  is thus required<sup>19</sup>. Therefore, an ON/OFF threshold value of 400 is used to define functional OECTs throughout this report, and this threshold was applied as the criterion to determine the manufacturing yield. All the 600 Small OECTs were operational and exhibited ON/OFF current ratios varying between 2200 (measured minimum value) and 32,000 (maximum value) with an empirical mean value of 7800. This demonstrates consistency of the screen printing process, and also indicates that it is possible to obtain similar switching functionality in all OECTs across the relatively large substrate. Notably, the lowest ON/OFF value obtained from the set of Small OECTs is 2200, which certainly is sufficient to guarantee successful propagation of a signal through cascaded sub-circuits in a screen-printed large-area OECT-based circuit. Thus, we classify all the 600 OECTs as operational, i.e., the manufacturing yield is here 100%.





**Fig. 3 OECT behavior.** **a** Transfer sweep of a block of Small OECTs (including five individual OECTs), **b** output curves of one Small OECT.



**Fig. 4 Histogram of the overall behavior of 600 Small OECTs.** **a** and **b** show the ON and OFF current distributions, **c** shows the distribution of the ON/OFF current ratio, **d** shows the distribution of the gate current in the OFF state.

Next, the performance parameters of the Large Version 1 and Large Version 2 OECTs were examined, especially paying attention to the effect of the size of the carbon areas exposed to the electrolyte. The transfer characteristics for these OECTs (Supplementary Fig. 1) indicate that there is a negative effect on the  $I_{D,OFF}$  and the  $I_{G,OFF}$  current levels as the area of the carbon contacts exposed to the electrolyte is increased.

In Fig. 5, the performance summary of the Large Version 1 and Large Version 2 OECTs is presented as histograms for the  $I_{D,ON}$ ,  $I_{D,OFF}$ ,  $I_{G,OFF}$  values and the drain current ON/OFF ratio for transfer curves recorded in the forward sweeps. Among the total of 160 large OECTs, there were only two of the Version 2 OECTs that were not functional, i.e., they were exhibiting an ON/OFF value below 400. (The microscope images of these two OECTs are shown in

Supplementary Fig. 2) These two malfunctioning OECTs are included when calculating the ON/OFF-based manufacturing yield for the printed sheet examined (the percentage of functional OECTs), but excluded from the performance statistics presented in Fig. 5. The empirical mean value of  $I_{D,ON}$  for all large OECTs, i.e., the 158 operational large OECTs, is  $-0.4$  mA whereas the mean value of  $I_{D,OFF}$  is  $-230$  nA and  $-500$  nA for the Large Version 1 and Large Version 2, respectively. Consequently, the empirical mean value of the ON/OFF current ratio for Large Version 1 and Large Version 2 OECTs is 2250 and 720, respectively. Based on these empirical mean values and the corresponding standard deviations, Gaussian distributions were plotted. As seen in Fig. 5, the two sets of large OECTs display two distinctly different, but closely situated,  $I_{D,ON}$  distributions with only 0.09 mA difference between their mean

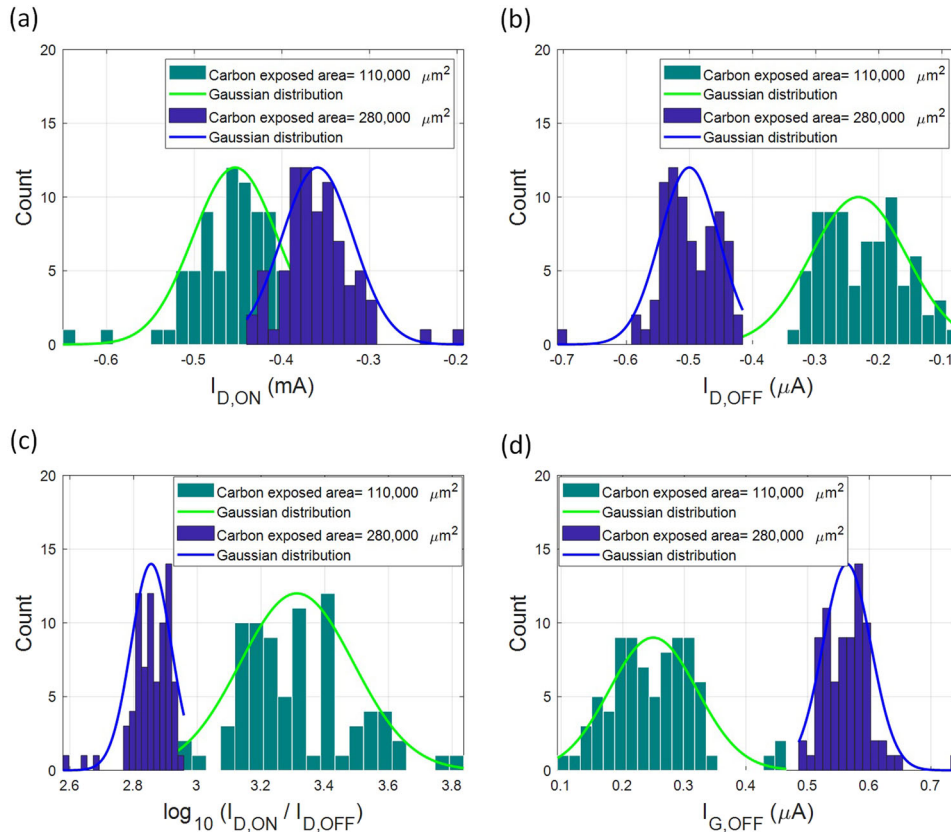


**Fig. 5** Histogram of the overall behavior of the two sets of large OECTs. **a** and **b** show the ON and OFF current distributions, **c** shows the ON/OFF current ratio distributions of 158 large OECTs, **d** shows the current distribution of the gate current in the OFF state.

values. This is due to that the active channel areas are identical for the two designs. However, a relatively much larger difference is found for the ON/OFF current ratios when comparing Large Version 1 and 2. The difference stems from the fact that the  $I_{D,OFF}$  values are not equal. We hypothesize that the different sizes of the carbon source and drain contact areas, exposed to the electrolyte, lead to different levels of parasitic electrochemical reactions. The most probable parasitic electrochemical reactions are associated with water splitting at the drain and/or the source electrodes at an elevated voltage difference between the gate electrode and the carbon pads serving as the drain and source electrodes. Upon applying a potential difference between the source and drain contacts, electrochemical side reaction is inevitable, and this effect should scale with the contact area exposed to the electrolyte (cf. Fig. 2b). So, for  $I_{G,OFF}$ ,  $I_{D,OFF}$ , and the ON/OFF current ratio two distinctive sets of Gaussian distributions are representing the Large Version 1 (green counts) and Large Version 2 (blue counts) OECTs, see Fig. 5. The minimum and maximum values of the ON/OFF current ratio for the 80 operational Large Version 1 OECTs are  $\sim 900$  and  $\sim 6900$ , respectively, with the empirical mean value of 2250. For the 78 operational Large Version 2 OECTs,  $\sim 400$  and  $\sim 900$  are the minimum and maximum ON/OFF values, respectively, with an empirical mean value of 720. From this comparison it is obvious that the Large Version 1 OECTs are superior as compared to the Large Version 2 OECTs. It is worth mentioning that even the lowest ON/OFF current ratio measured (400, as obtained from the Large Version 2 OECTs) most probably will work in an OECT-based circuit where a minimum ON/OFF current ratio of  $\sim 400$  is required.

All three OECT structures (Small, Large Version 1, Large Version 2) exhibit more or less the same  $I_{D,ON}$  values ( $-0.4$  mA) and related distributions (cf. Figs. 4a and 5a) due to identical channel resistor values, which stems from the fact that all

**Table 1.** Summary of the ON/OFF current ratio for the three OECT structures.

OECT structure	Number of OECTs	Mean value	Maximum value	Minimum value
Small	600	7800	$\sim 32,000$	$\sim 2200$
Large Version 1	80	2250	$\sim 6900$	$\sim 900$
Large Version 2	78	720	$\sim 900$	$\sim 400$

channels are shaped as squares, making the channel resistance equal to the PEDOT:PSS sheet resistance of  $\sim 1$  k $\Omega/\square$ . Furthermore, it can be observed that enlarging the OECT channel and the carbon area exposed to the electrolyte by a factor of four (Small vs. Large Version 2 OECTs) results in significantly increased  $I_{D,OFF}$  values. The empirical mean value of  $I_{D,OFF}$  for the Small OECTs and Large Version 2 OECTs is  $-70$  and  $-500$  nA, respectively. In Table 1, empirical mean, minimum, and maximum values of the ON/OFF current ratios of the three OECT structures are summarized. Following the assumption of having an ON/OFF ratio threshold value of  $\sim 400$  to define the manufacturing yield, all 600 Small OECTs are positioned well above this limit. Although the large OECTs were designed for the purpose of studying the effect of the carbon areas exposed to the electrolyte, they also satisfy the assumption. The overall manufacturing yield of the 760 OECTs is 99.7% with only two malfunctioning OECTs.

When applying printed OECTs into various applications, such as in digital switches and circuits, the dynamic switching characteristics is of importance. In the dynamic switching tests conducted here,  $V_G$  was sourced from a function generator in the form of a square wave alternating between 0 and 1.5 V at 500 MHz frequency, with a 50% duty cycle, and at the same time a

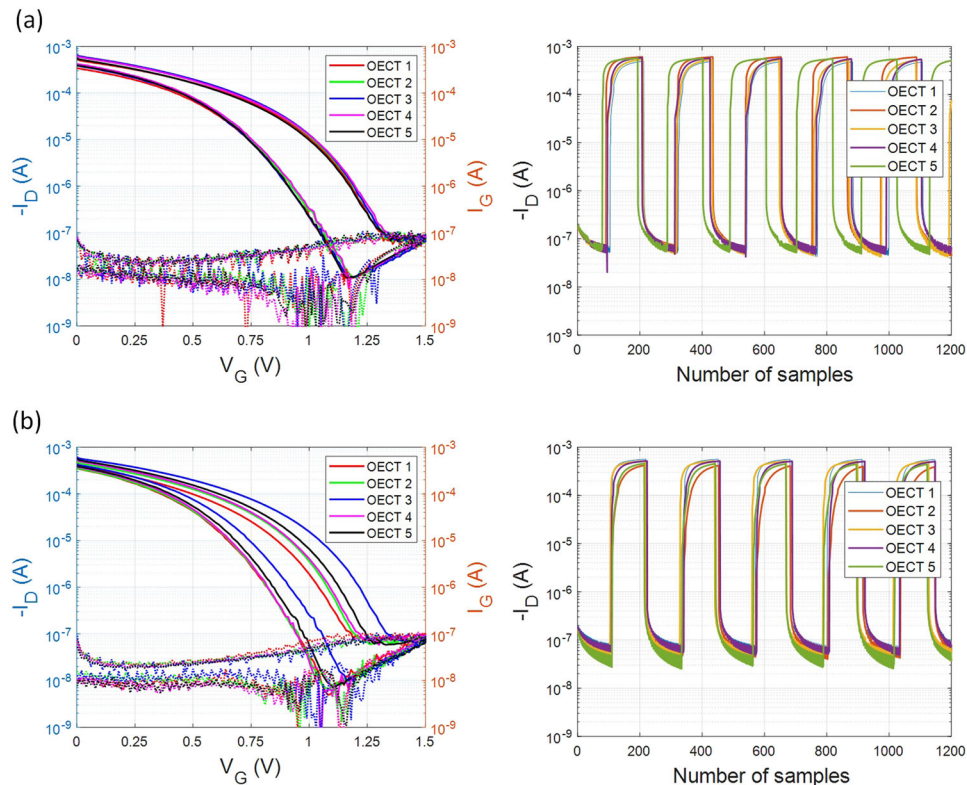


**Fig. 6 Dynamic switching behavior of two blocks of Small OECTs along with their transfer measurements.** **a** Dynamic switching of a Small OECT block with matching transfer curves, **b** dynamic switching of a Small OECT block with varying transfer curves. Despite the variations in transfer characteristics, the ON/OFF current ratios that are obtained are identical (both showing  $I_{D,ON}$  and  $I_{D,OFF}$  of  $\sim 400 \mu\text{A}$  and  $\sim 30 \text{nA}$ , respectively), which is an important result from a circuit design perspective.

constant  $V_D$  of  $-1 \text{ V}$  was applied.  $I_D$  was then measured using an integration time of  $640 \mu\text{s}$ . Figure 6 displays the dynamic switching characteristics of two blocks of Small OECTs along with their corresponding transfer characteristics. In the dynamic switching tests, the cycle time was set to  $2 \text{ s}$ . The sampling frequency differs slightly from sample to sample due to limitations of the parameter analyzer (*HP/Agilent 4155B*) and therefore the time axis of each curve has been normalized with respect to its sampling frequency. The two Small OECT blocks were selected in a manner that the transfer curves of all the OECTs within one block either match very well with one another (cf. Fig. 6a) or differ significantly from each other (cf. Fig. 6b). It is observed that the dynamic switching behavior is consistent regardless if the transfer curves are overlapping or not. This is due to the fact that the  $I_{D,ON}$  and  $I_{D,OFF}$  levels are almost identical for the transfer curves even when the different transfer curves do not overlap. Based on these results, the fabricated OECTs, here reported, are found to be good candidates for future development of digital circuits of various kinds, mainly due to that maximum ON/OFF current ratio is obtained even with slight variations in transfer characteristics.

The switching time is one of the key parameters in printed circuit applications, as it dictates the overall speed of circuit operation. For OECTs, the switching times typically fall in the  $20$  to  $200 \text{ ms}$  range<sup>5,21</sup>. For the Small OECTs, here presented in Fig. 6, the typical switching times for ON-to-OFF ( $I_D$  switches from 90 to 10% of its maximum value), and OFF-to-ON ( $I_D$  switches from 10 to 90% of its maximum value), extracted from the dynamic switch measurements, are found to be  $20$  and  $225 \text{ ms}$ , respectively (dynamic switching measurements of the two large versions of OECTs are provided in Supplementary Fig. 1). The Large Version 1 OECT gives higher current modulation than the Large Version 2. For Large Version 1 OECTs, the typical switching times for ON-to-

OFF and OFF-to-ON are found to be  $240 \text{ ms}$  and  $1.4 \text{ s}$ , respectively. The ON-to-OFF and OFF-to-ON switching times for Large Version 2 OECTs are  $320 \text{ ms}$  and  $1.8 \text{ s}$ , respectively. The Small OECTs exhibit the shortest switching times due to their small channel area along with their small carbon areas exposed to the electrolyte. Comparing the two sets of large OECT versions, the switching time is prolonged as the carbon areas exposed to the electrolyte are increased.

#### Miniaturization

Because of the excellent manufacturing yield and performance of the Small OECTs, additional miniaturization steps were undertaken, in order to further push the limits of OECTs manufactured by screen printing. OECTs with channel dimensions of  $150 \times 100 \mu\text{m}^2$  and carbon areas exposed to the electrolyte of  $45,000 \mu\text{m}^2$  were designed and printed, referred to as Tiny OECTs. The performance of the Tiny OECTs was evaluated based on drain current ON/OFF ratios. While promising results were achieved for some of the OECTs in this design, precision limitations of the printing method frequently came into play at these dimensions and the results were not entirely consistent.

ON/OFF current ratios higher than  $100,000$  were observed for some of these OECTs. As an example, the performance of a block of six printed OECTs (Supplementary Fig. 3a) gives  $I_{D,ON}$  and  $I_{D,OFF}$  values of  $\sim 1 \text{ mA}$  and  $\sim 5 \text{ nA}$ , respectively. The relatively higher  $I_{D,ON}$ , as compared to the values reported above, is explained by that the channel length and width are  $100$  and  $150 \mu\text{m}$ , respectively, which results in a lower channel resistance value than for the square-shaped channels. Further, the Tiny OECT design has also a smaller carbon area exposed to the electrolyte, which leads to relatively lower parasitic current contribution, and



hence lower values of  $I_{D,OFF}$  and  $I_{G,OFF}$ . This led to ON/OFF current ratios of more than five orders of magnitude. However, the results in terms of  $I_{D,ON}$  and  $I_{D,OFF}$  levels were not consistent for the entire sheet and the manufacturing yield in terms of ON/OFF current ratio decreased to about 98% (based on the yield threshold of ON/OFF current ratio  $> 400$ ). The reason for the decreased yield is probably directly tied to the small dimensions used, which introduces more malfunctioning devices. Printing several consecutive layers on top of each other requires excellent alignment accuracy between all the different layers. When the printed dimensions are truly small with respect to the accuracy limitation of the printing method, even a slight misalignment will have detrimental impact on the performance of the printed OECT device. Unintended contacts between layers will affect the performance, leading to large spread in terms of ON/OFF current ratio (exemplified in Supplementary Fig. 3b) across the sheet, or even inoperative devices, both being equally bad from a circuit design perspective. For instance, having an insulator layer slightly misaligned with respect to the carbon pads (serving as the source and drain electrodes) may create a different OECT architecture, and hence utterly different switching performance<sup>22</sup>. Having this in mind, it is critical to ensure that the same type of OECT architecture can be printed across the whole substrate area; hence, screen printing of the smallest possible OECT structures is not recommended. Choosing the Small OECT design results in more reliable and reproducible devices and is preferable over the Tiny OECT design, even though the trade-off leads to higher leakage current and lower ON/OFF current ratio.

## DISCUSSION

In total, four different fully screen-printed OECT structures have been manufactured using six (as shown in Fig. 2a) different layers. The performance of the printed OECTs in terms of ON/OFF current ratio has been reported. The manufacturing yield has been defined and studied as the percentage of functional OECTs (ON/OFF current ratio  $> 400$ ). For Small OECTs, we observed that the empirical ON/OFF current ratios of all devices range from 2200 to 32,000. For Large Version 1 OECTs, the ON/OFF current ratios range from 900 to 6900. Finally, for Large Version 2 OECTs, the ON/OFF current ratios range from  $\sim 400$  to  $\sim 900$ . The results demonstrate that OECTs with large carbon areas exposed to the electrolyte give higher leakage current and lower ON/OFF current ratios. The overall manufacturing yield of the 760 OECTs reached an impressive level of 99.7%; only two OECTs were inoperative. The ON/OFF current ratios of the 758 operational OECTs ranged from 2.6 to 4.5 orders of magnitude. The dynamic switching tests also showed consistent behavior. This indicates the potential of using screen printing as a low cost and large-scale production method to create printed electronic devices and circuits with high manufacturing yield. With sufficiently small size, the screen-printed OECTs are appropriate candidates for developing reproducible complex printed logic circuits on large-area substrates (A4 size). OECTs with channel dimensions of  $150 \times 100 \mu\text{m}^2$  and a carbon area of  $45,000 \mu\text{m}^2$  in direct contact with the electrolyte were also developed and evaluated. For these devices, referred to as the Tiny OECT design, the ON/OFF current ratio can exceed 100,000; however, the results were less consistent throughout the sheet and the manufacturing yield was lowered to 98%. Such manufacturing yield might be sufficient for standalone transistors or logical elements, but probably not for printed circuitry. Hence, there is a trade-off between performance and manufacturing yield of printed OECTs, but with the accuracy obtainable with screen printing, good and useful transistors can be produced with very high manufacturing yield.

## METHODS

### OECTs fabrication

The OECT layouts were designed in the Clewin software (*WieWeb Software Inc., Netherlands*). All printing was carried out under ambient conditions. All materials were printed on top of a flexible PET plastic substrate by using a flatbed sheet-fed screen printer (*DEK Horizon 03ix*). PET is one of the most common substrates in printed electronics. It is thin and flexible, compatible with printing technologies, and commercially available in large quantities at low cost. Standard polyester meshes have been applied for the screen printing process. As the first step, silver ink (*Ag 5000* purchased from *DuPont*) was printed on top of the flexible PET substrate to create the probing contact pads. Then a PEDOT:PSS (*Clevios SV4* purchased from *Heraeus*) stripe was deposited between the outer silver pads, serving as the electrochemically active transistor channel. In the next step, carbon electrodes (*7102* conducting screen printing paste purchased from *DuPont*) were patterned at the ends of the deposited PEDOT:PSS channel stripe. Each of these first three layers was followed by an annealing step in a conveyor belt oven at  $120^\circ\text{C}$  for 5 min. Thereafter, a pattern of insulating material (*5018* purchased from *DuPont*) was deposited, followed by UV-curing. Subsequently, the open area defined by the insulating layer was filled by screen printing an electrolyte ink based on poly(diallyldimethylammonium chloride) dissolved in water (*AFI VV009* provided by *RISE Acreo*), followed by UV-curing to transform it into a solid electrolyte layer. Hence, the PEDOT:PSS stripe in direct contact with the electrolyte layer serves as the active channel of the OECT. To finalize the device, a PEDOT:PSS layer is printed on top of the electrolyte layer to form the gate electrode. Figure 1 depicts the printed test structures including a microscope image of a single OECT and a cross-sectional schematic depicting the different layers of a screen-printed OECT. From a functionality point of view, the thickness is a non-critical parameter for most of the printed layers in an OECT. Owing to this, no optimization with respect to thickness has been performed in this work, and the following thicknesses were estimated by using a *Sensofar PLu neox* optical profilometer after screen printing the different layers on a PET substrate: carbon  $9 \mu\text{m}$ , silver  $11 \mu\text{m}$ , insulator  $15 \mu\text{m}$ , and electrolyte  $13 \mu\text{m}$ . The thickness and uniformity of the PEDOT:PSS serving as the OECT channel have, however, an impact on the device switching performance. The thickness and roughness of this layer were  $0.5 \mu\text{m}$  and  $30 \text{nm}$ , respectively, and such a thin and uniform layer enables reproducible devices with relatively short switching times.

### Electrical characterization

In order to attain comparable results, all samples were stored and measured in a controlled environment at  $\sim 20^\circ\text{C}$  and  $\sim 50\%$  relative humidity (RH). Transfer (drain current vs. gate voltage), output (drain current vs. drain voltage), and dynamic switching (drain current vs. time) measurements were carried out using a semiconductor parameter analyzer (*HP/Agilent 4155B*) and a function generator (*Agilent 33120A*). The following notation is used: the voltage between the drain and the source is denoted  $V_D$ ; the voltage between the gate and the source is denoted  $V_G$ ; in the forward sweep of the transfer measurements, the drain current values at  $V_G = 100 \text{mV}$  and at  $V_G = 1.5 \text{V}$  are denoted  $I_{D,ON}$  and  $I_{D,OFF}$ , respectively; in the dynamic measurements, the drain current values at  $V_G = 0 \text{V}$  and at  $V_G = 1.5 \text{V}$  are denoted  $I_{D,ON}$  and  $I_{D,OFF}$ , respectively.

## DATA AVAILABILITY

The data that support the findings of this study are available from the corresponding author upon reasonable request.

Received: 30 October 2019; Accepted: 3 June 2020;

Published online: 03 August 2020

## REFERENCES

- Søndergaard, R. R., Hösel, M. & Krebs, F. C. Roll-to-roll fabrication of large area functional organic materials. *J. Polym. Sci. B. Polym. Phys.* **51**, 16–34 (2013).
- Breggren, M. et al. Browsing the real world using organic electronics, Si-Chips, and a human touch. *Adv. Mater.* **28**, 1911–1916 (2016).

3. Hütter, P. C., Rothlander, T., Scheipl, G. & Stadlober, B. All screen-printed logic gates based on organic electrochemical transistors. *IEEE Trans. Electron Devices* **62**, 4231–4236 (2015).
4. Hütter, P. C., Fian, A., Gatterer, K. & Stadlober, B. Efficiency of the switching process in organic electrochemical transistors. *ACS Appl. Mater. Interfaces* **8**, 14071–14076 (2016).
5. Andersson Ersman, P. et al. Screen printed digital circuits based on vertical organic electrochemical transistors. *Flex. Print. Electron.* **2**, 45008 (2017).
6. Hyun, W. J., Secor, E. B., Hersam, M. C., Frisbie, C. D. & Francis, L. F. High-resolution patterning of graphene by screen printing with a silicon stencil for highly flexible printed electronics. *Adv. Mater.* **27**, 109–115 (2015).
7. Mandal, S. & Noh, Y. Y. Printed organic thin-film transistor-based integrated circuits. *Semicond. Sci. Technol.* **30**, 1–20 (2015).
8. Rivnay, J. et al. Organic electrochemical transistors. *Nat. Rev. Mater.* **3**, 17086 (2018).
9. Kittlesen, G. P., White, H. S. & Wrighton, M. S. Chemical derivatization of microelectrode arrays by oxidation of pyrrole and N-methylpyrrole: fabrication of molecule-based electronic devices. *J. Am. Chem. Soc.* **106**, 7389–7396 (1984).
10. Shirinskaya, A., Horowitz, G., Rivnay, J., Malliaras, G. & Bonnassieux, Y. Numerical modeling of an organic electrochemical transistor. *Biosensors* **8**, 103 (2018).
11. Zirkel, M. et al. An all-printed ferroelectric active matrix sensor network based on only five functional materials forming a touchless control interface. *Adv. Mater.* **23**, 2069–2074 (2011).
12. Hamed, M., Forchheimer, R. & Inganäs, O. Towards woven logic from organic electronic fibres. *Nat. Mater.* **6**, 357–362 (2007).
13. Andersson Ersman, P., Forchheimer, R., Tehrani, P. & Berggren, M. Printable all-organic electrochromic active-matrix displays. *Adv. Funct. Mater.* **17**, 3074–3082 (2007).
14. Gerasimov, J. Y. et al. An evolvable organic electrochemical transistor for neuromorphic applications. *Adv. Sci.* **6**, 1801339 (2019).
15. Diacci, C. et al. Real-time monitoring of glucose export from isolated chloroplasts using an organic electrochemical transistor. *Adv. Mater. Technol.* **0**, 1900262 (2019).
16. Lee, W. & Someya, T. Emerging trends in flexible active multielectrode arrays. *Chem. Mater.* **31**, 6347–6358 (2019).
17. Sowade, E. et al. Up-scaling of the manufacturing of all-inkjet-printed organic thin-film transistors: Device performance and manufacturing yield of transistor arrays. *Org. Electron.* **30**, 237–246 (2016).
18. Sowade, E. et al. All-inkjet-printed thin-film transistors: Manufacturing process reliability by root cause analysis. *Sci. Rep.* **6**, 1–15 (2016).
19. Savva, A. et al. Influence of water on the performance of organic electrochemical transistors. *Chem. Mater.* **31**, 927–937 (2019).
20. Andersson Ersman, P. et al. All-printed large-scale integrated circuits based on organic electrochemical transistors. *Nat. Commun.* **10**, 5053 (2019).
21. Blaudeck, T. et al. Simplified large-area manufacturing of organic electrochemical transistors combining printing and a self-aligning laser ablation step. *Adv. Funct. Mater.* **22**, 2939–2948 (2012).
22. Andersson Ersman, P., Nilsson, D., Kawahara, J., Gustafsson, G. & Berggren, M. Fast-switching all-printed organic electrochemical transistors. *Org. Electron. Phys. Mater. Appl.* **14**, 1276–1280 (2013).

## ACKNOWLEDGEMENTS

This work was primarily supported by the Swedish foundation for Strategic Research (Silicon-Organic Hybrid Autarkic Systems, Reference number: SE13-0045). Additional support was provided by the Knut and Alice Wallenberg Foundation (Wallenberg Wood Science Center and Wallenberg Scholars). Open access funding provided by Linköping University.

## AUTHOR CONTRIBUTIONS

P.A.E., I.E., and M.B. conceived the research idea. J.S. fabricated devices with assistance from M.Z. based on design input from P.A.E., M.Z., and R.L. M.Z. characterized the devices. P.A.E., I.E., R.L., M.B., and S.F. supervised the research. M.Z. wrote the paper with contributions from all authors.

## COMPETING INTERESTS

The authors declare no competing interests.

## ADDITIONAL INFORMATION

**Supplementary information** is available for this paper at <https://doi.org/10.1038/s41528-020-0078-9>.

**Correspondence** and requests for materials should be addressed to I.E.

**Reprints and permission information** is available at <http://www.nature.com/reprints>

**Publisher's note** Springer Nature remains neutral with regard to jurisdictional claims in published maps and institutional affiliations.



**Open Access** This article is licensed under a Creative Commons Attribution 4.0 International License, which permits use, sharing, adaptation, distribution and reproduction in any medium or format, as long as you give appropriate credit to the original author(s) and the source, provide a link to the Creative Commons license, and indicate if changes were made. The images or other third party material in this article are included in the article's Creative Commons license, unless indicated otherwise in a credit line to the material. If material is not included in the article's Creative Commons license and your intended use is not permitted by statutory regulation or exceeds the permitted use, you will need to obtain permission directly from the copyright holder. To view a copy of this license, visit <http://creativecommons.org/licenses/by/4.0/>.

© The Author(s) 2020